Asian Journal of Pharmaceutical Sciences 16 (2021) 459–470

Available online at www.sciencedirect.com

ScienceDirect

journal homepage: www.elsevier.com/locate/AJPS

Original Research Paper

Macrophage membrane-mediated targeted drug delivery for treatment of spinal cord injury regardless of the macrophage polarization states

*Wei Tang, Yi Yang, Ling Yang, Mei Tang, Ying Chen, Chong Li**

Medical Research Institute, College of Pharmaceutical Sciences, Southwest University, Chongqing 400715, China

ARTICLE INFO

Article history:
Received 14 January 2021
Revised 4 March 2021
Accepted 30 March 2021
Available online 29 April 2021

Keywords:
Spinal cord injury
Pyroptosis
Macrophage polarization
Minocycline
Actively targeted delivery

ABSTRACT

Targeted delivery of therapeutics for spinal cord injury (SCI) has been a long-term challenge due to the complexity of the pathological procession. Macrophage, as an immune cell, can selectively accumulate at the trauma site after SCI. This intrinsic targeting, coupled with good immune-escaping capacity makes macrophages an ideal source of biomimetic delivery carrier for SCI. Worth mentioning, macrophages have multiple polarization states, which may not be ignored when designing macrophage-based delivery systems. Herein, we fabricated macrophage membrane-camouflaged liposomes (RM-LIPs) and evaluated their abilities to extend drug circulation time and target the injured spinal cord. Specially, we detected the expression levels of the two main targeted receptors Mac-1 and integrin α4 in three macrophage subtypes, including unactivated (M0) macrophages, classically activated (M1) macrophages and alternatively activated (M2) macrophages, and compared targeting of these macrophage membrane-coated nanoparticles for SCI. The macrophage membrane camouflage decreased cellular uptake of liposomes in RAW264.7 immune cells and strengthened binding of the nanoparticle to the damaged endothelial cells *in vitro*. RM-LIPs can prolong drug circulation time and actively accumulate at the trauma site of the spinal cord *in vivo*. Besides, RM-LIPs loaded with minocycline (RM-LIP/MC) showed a comprehensive therapeutic effect on SCI mice, and the anti-pyroptosis was found to be a novel mechanism of RM-LIP/MC treatment of SCI. Moreover, the levels of Mac-1 and integrin α4 in macrophages and the targeting of RM-LIP for SCI were found to be independent of macrophage polarization states. Our study provided a biomimetic strategy via the biological properties of macrophages for SCI targeting and treatment.

* Corresponding author.
E-mail address: chongli@swu.edu.cn (C. Li).
Peer review under responsibility of Shenyang Pharmaceutical University.

https://doi.org/10.1016/j.ajps.2021.03.005

1. Introduction

Spinal cord injury (SCI) is a common neurological disease that affects more than 180000 individuals each year worldwide [1]. The motor and sensory dysfunctions due to SCI seriously affect the quality of life of patients and also bring a heavy financial and medical burden on society [2]. Most spinal cord trauma cases involve two phases: primary injury and secondary injury [3]. Different from the primary injury, which is immediate and beyond therapeutic management, the secondary injury occurs over the hours and days after SCI, which further exacerbates tissue loss and functional impairments, and is the main obstacle to the recovery of kinematic function after SCI [1,4]. At present, only a few drugs such as methylprednisolone and minocycline can be used for secondary injury after SCI [5–7]. However, due to the lacking specific targeting, it is difficult to deliver a sufficient amount of these agents to the damaged site by traditional delivery route without significant side-effects, thus effective therapy for SCI remains a great challenge.

Recently, biomimetic-nanoparticle delivery systems (BNP-DSs) are gaining attention [8]. By transferring bioactive cellular components to the surface of synthetic particles, BNP-DSs not only retain good physical properties of conventional nanoparticles, but also have unique biological functions of the biological entities, such as active targeting potency and high biocompatibility [9–11]. For example, erythrocyte membrane-camouflaged polymeric nanoparticles showed superior circulation half-life in mice [12]. Cancer cell membrane-coated nanoparticles demonstrated specific homologous targeting to cancer cells [13]. Platelet membrane-cloaked nanoparticles had selective adhesion to damaged vasculatures [14]. During secondary spinal cord injury, macrophages, as a kind of immune cell, can be recruited, roll on the impaired microvascular endothelium and penetrate into the spinal cord injured sites [15]. The interaction between integrin $\alpha 4$ and Mac-1 on the macrophage membranes and vascular cell adhesion molecule-1 (VCAM-1) on impaired microvascular endothelium is one of the main mechanisms of macrophages accumulating at the trauma site after SCI [16]. Therefore, it is possible that developing macrophage membrane-camouflaged nanoparticles for targeting SCI, which could delay uptake by the mononuclear phagocyte system and actively accumulate at the trauma site, thus more effectively deliver drugs to the injured spinal cord.

Different from red blood cells, tumor cells, etc., macrophages can change their morphology and physiological function to respond to environmental stimuli, which has been referred to as macrophage polarization [17]. Macrophages have two major polarization states: classically activated M1 macrophages and alternative-activated M2 phenotypes [18]. Nie et al. chose specially to use M1 phenotype macrophage exosomes induced by Mn^{2+} for targeted tumor delivery to improve the therapeutic effect [19]. Wang et al. designed a kind of bacteria-pretreated macrophage-membrane coating gold-silver nanoparticle and confirmed it had better bacterial targeting compared with untreated macrophage-membrane coating nanoparticle [20]. Therefore, the influence of macrophage polarization states may not be ignored when designing macrophage-based delivery systems.

Herein, we explore the use of RAW246.7 cells membrane decorated liposomes (RM-LIP) for SCI targeting and treatment. Firstly, we characterized the physicochemical properties and biological features of RM-LIP. Then, the capacity of RM-LIP to prolong drug circulation time and target the injured site after SCI was confirmed using a combination of *in vitro* and *in vivo* experiments. In addition, the expression levels of two significant target receptors on three different macrophage subtypes were measured by using an absolute quantitative method, and targeting of these macrophage membrane-coated nanoparticles also were evaluated. Finally, the therapeutic efficacy of minocycline-loaded RM-LIP (RM-LIP/MC) was assessed in an SCI mouse model, and the anti-pyroptosis as a novel treatment mechanism was confirmed. Additionally, the safety of the RM-LIP/MC was also preliminarily examined.

2. Materials and methods

2.1. Materials

Egg Phosphatidylcholine (EPC), Cholesterol (Cho) and $mPEG_{2000}$-DSPEwere purchased from A.V.T. Pharmaceutical Co., Ltd. (China). Minocycline hydrochloride (MC) was supplied by Bide Pharmatech Ltd. (China). purchased from Aladdin Biochemical Technology Co., Ltd. (China). IFNγ and IL-4 were provided by Beyotime Biotechnology Co., Ltd. (China). DAPI, DiIC18(3) (DiI), DiIC18(5) (DiD) and DiIC18(7) (DiR) were supplied by US Everbright Inc. (China). Lipopolysaccharide (LPS), nile red (NiL) and coumarin 6(C6) were provided by Aladdin Co., Ltd. (China). VCAM-1 rabbit Ab, GFAP rabbit Ab and Goat Anti-rabbit IgG Ab were supplied by BiossBiotechnology co. LTD (China). NF-H rabbit Ab was obtained from Gene Tex. (USA). Anti-Mac-1,anti-integrin $\alpha 4$, anti-NLRP3, anti-Caspase-1, anti-ASC, anti-GSDMD, CoraLite488-labeled goat anti-rabbit IgG(H+L) and Cy3-conjugated goat anti-rabbit IgG(H+L) were purchased from Proteintech Group, Inc (USA). Rabbit anti-GSDMD-N Ab was supplied by Abcam (UK). Mouse TNF-α and IL-6 enzyme-linked immunosorbent assay (ELISA) kits were purchased from Shanghai Enzyme-linked Biotechnology Co., Ltd (China), PE anti-Mac-1 antibody Human IL-1β and IL-18 ELISA kits were supplied by Jingmei Biotechnology Co., Ltd. (China). Quantum^{TM}R-PE MESF Kit was obtained from Bangs Laboratories, Inc.(USA). Murine monocyte macrophage cell line (RAW264.7) and human umbilical vein endothelial cell line (HUVEC) were provided by the Cell Bank of the Chinese Academy of Sciences (Shanghai, China). All animal experiments were approved by the experimental animal ethics committee of College of Pharmaceutical Sciences, Southwest University.

2.2. Preparation of RM-LIP

The macrophage membrane was isolated from RAW 264.7 cells as previously described [21]. Minocycline liposomes (MC-LIP) were prepared by the Calcium acetate gradient method

[22]. Briefly, a lipid film composed of PC and Cho (molar ratio, 7:3) was prepared in a round-bottom flask by removing chloroform from lipid solution. The dried lipid film was further hydrated with 120 mM $CaCl_2$, 120 mM CH_3COONa at 37°C for 30 min up to a final liposome concentration of 10 mg/ml. The suspension was ultrasonicated under an ice water bath to prepare blank liposomes and unencapsulated $CaCl_2$ and CH_3COONa were removed by dialysis for 1 h. To 1 ml liposomal formulation, 3 mg minocycline was added and was incubated at 40 °C for 15 min.

Various fluorescent liposomes in the article were prepared by a thin-film hydration method [23]. In brief, PC and Cho (molar ratio,7:3) were mixed in chloroform-methanol (1:1; v/v), and then the nile red, C6, DiI or DiR were added at a concentration of 10 μg Nile Red per 10 mg PC, 10 μg C6 per 10 mg PC, 10 μg DiI per 10 mg PC, 50 μg DiR per 10 mg PC, respectively. The lipid solution was rotary-evaporated to form a lipid film, and was hydrated with the 5% glucose solution at 37 °C and finally ultrasonicated under an ice water bath to form liposomes. PEGylatedminocycline liposomes (PEG-LIP/MC) and fluorescent probe liposomes (PEG-LIP) were prepared by a similar process as related control liposomes (LIP), except the materials consisted of PC, Cho and $mPEG_{2000}$-DSPE (molar ratio, 7:3:0.35).RM-LIP was fabricated by an extrusion method [21,24]. The purified macrophage membrane from 1×10^8 cells was mixed with 1 ml of minocycline-loaded PEG-LIP and sequentially extruded through a polycarbonate membrane with pore sizes of 400,200 and 100 nm for 20 times respectively to prepare RM-LIP/MC.

2.3. Characterization of the RM-LIP

The particle size and zeta potential of RM-LIP were measured by dynamic light scattering (DLS) (Nano ZS, Malvern, UK), and the morphology of RM-LIP was shown directly using a transmission electron microscope (TEM) (HITACHI, HT7800, Japan). The average particle sizes of RM-LIP in 5% glucose solution were tested at different time points within 72 h at 37 °C to evaluate its stability over time. PEG-LIP served as a control in the above experiments. For fluorescent co-localization analysis, liposomes were labeled with C6, while RAW264.7 membranes were labeled with DiI. The fluorescent-labeled samples were imaged by a 63 × objective on a high-content analysis system (HCS) (PerkinElmer, Operetta CLS, USA).

To detect the drug encapsulation efficiency (EE) of the RM-LIP/MC, free minocycline was removed with a Sephadex G-50 gel filtration column, encapsulated minocycline was detected by HPLC (Shimadzu, LC-20AD, Japan) at a wavelength of 280 nm. The calculated formula of EE as follows:

$$EE\,(\%) = \frac{\text{Minocycline encapsulated in RAW} - \text{LIP / MC}}{\text{Total minocycline}} \times 100\%$$

The protein profiles of the RM-LIP were preliminarily determined by sodium dodecyl sulfate-polyacrylamide gel electrophoresis (SDS-PAGE). Briefly, RAW264.7 membrane and RM-LIP firstly were treated with RIPA lysis buffer, and mixed in SDS sample buffer and heated at 100 °C for 10 min. The protein concentration in the lysates was determined by using a BCA Protein Assay Kit. Then, each sample was separated by electrophoresis on a 10% sodium dodecyl sulfate-polyacrylamide gel and was stained with Coomassie Brilliant Blue before imaging. In addition, the liposome without membrane was performed as a control. The expression of integrin α4 and Mac-1 in RAW 264.7, RAW 264.7 membrane and RM-LIP, and the level of VCAM-1 in HUVEC were analyzed by Western blot. First, samples underwent electrophoresis and were transferred to the PVDF membrane. Next, the membrane was blocked by 5% skimmed milk powder at 37°C for 1 h. Then membranes were incubated overnight at 4 °C with corresponding primary antibody: rabbit anti-integrin α4 (1:1000, dilution), rabbit anti-Mac-1 (1:1000, dilution), and followed with by secondary antibody. The protein signals were detected with a chemiluminescence imaging system (General Electric Company, Boston, MA, USA). The protein signals of β-actin and Na^+/K^+-ATPase were measured as controls.

2.4. In vitro drug release

Freshly prepared minocycline-loaded liposomes were placed into dialysis bags (MWCO: 10000 Da) with release media (PBS) under continuous shaking at 37 °C. At predetermined time intervals, aliquots were withdrawn and replaced with an equal volume of fresh medium. Minocycline in the release medium was measured by HPLC, and the release profile of minocycline was plotted.

2.5. Anti-phagocytosis in vitro

Approximately 2×10^5 RAW264.7 cells were seeded in 12-well plates and cultured overnight. The NiL-labeled liposomes were added to the plates, incubated with cells for 1 h at 37 °C, and washed 3 times with cold PBS to remove liposomes that were not internalized. Nuclei were stained with DAPI for imaging under a confocal laser-scanning microscope (CLSM) (Leica TCS SP5, Germany). At the same time, cells were collected for flow cytometric analysis using FACS (BD Calibur, BD Biosciences, USA).

2.6. In vitro binding of RM-LIP to inflamed endothelium

To clarify the possible active targeting of RM-LIP, a binding experiment *in vitro* was executed using HUVECs. Firstly, HUVECs were implanted in 12-well plates and cultured. After the cells reached 50%–60% confluence, LPS (1 μg/ml) was added to the HUVECs culture and incubated for 24 h to establish an inflamed model. Then, NiL-labeled liposomes were added to the plates, cultured for 4 h at 4 °C, and then washed 3 times with cold PBS. The fluorescence intensities of the cells were quantified by the FACS. Meanwhile, the nuclei were stained with DAPI for visualization under the CLSM. The blocked RM-LIP, which was prepared by adding 20 μl anti-integrin α4 antibody and 20 μl anti-Mac-1 antibody to 1 ml of RM-LIP, also was set to verify the biomimetic function of RM-LIP. The binding test of liposomes to normal HUVECs was performed as a negative control.

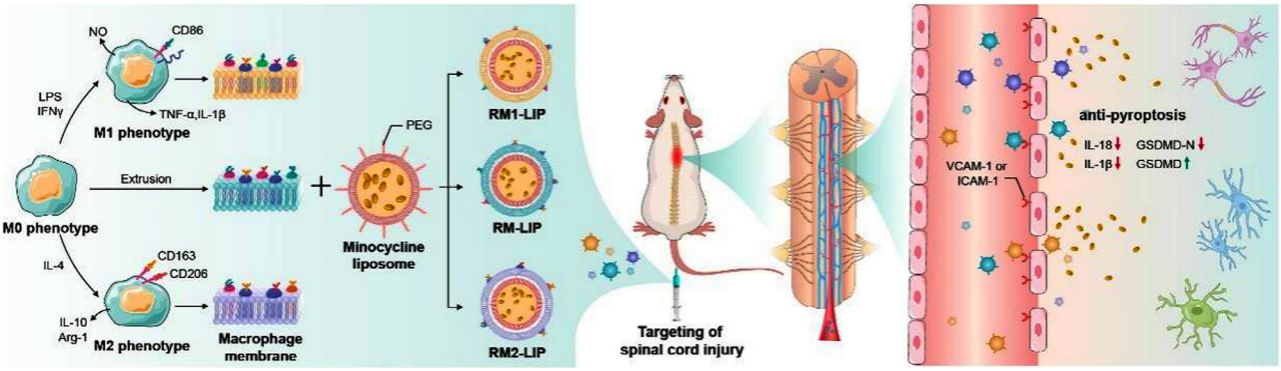

Fig. 1 – Schematic illustration depicting that different polarized macrophage membranes camouflaged nanoparticles actively target the injured spinal cord through receptor-ligand interactions, and the minocycline delivered to the injury site by RM-LIP exhibits a new treatment mechanism for spinal cord injury.

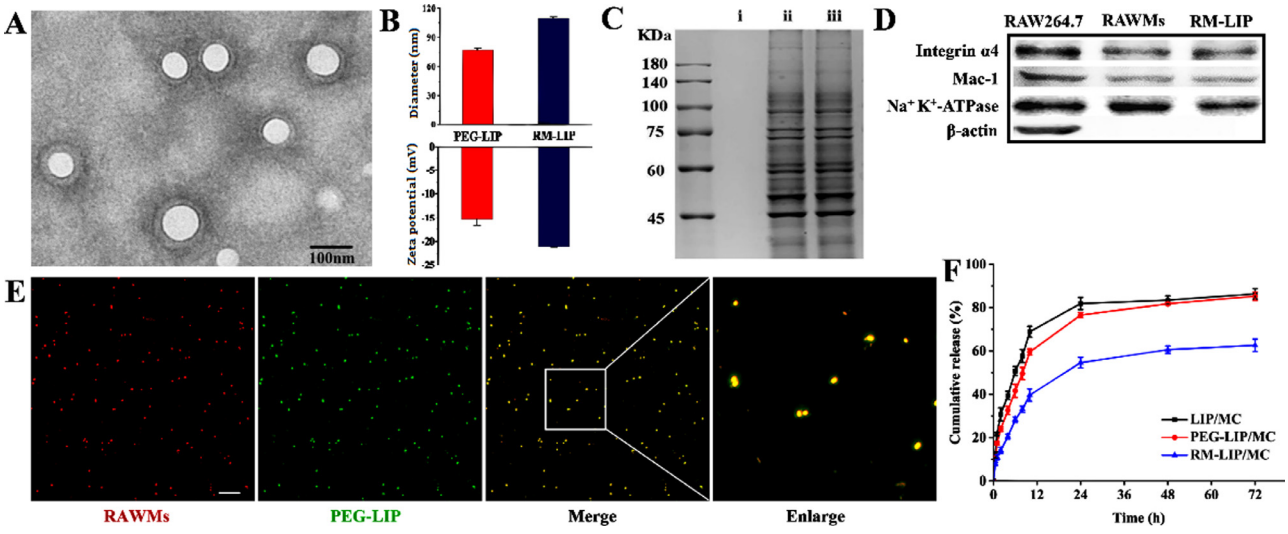

Fig. 2 – Characterization of RM-LIP. (A) TEM image of RM-LIP. scale bar, 100 nm.; (B) Size distribution and zeta potential of RM-LIP and PEG-LIP ($n = 3$); (C) Protein content of (i) PEG-LIP, (ii) RAWMs, (iii) RM-LIP, as analyzed by SDS-PAGE, protein marker shown in the left column; (D) Western blots of integrin α4 and Mac-1 in RAW264.7, RAWMs and RM-LIP, and Na^+K^+-ATPase and β-actin as internal reference proteins; (E) Co-localization of RAWMs (red) and PEG-LIP (green) by CLSM (scale bar: 5 μm). (F) Release profile of LIP/MC, PEG-LIP/MC and RM-LIP/MC in PBS at 37 °C ($n = 3$).

2.7. *Ex vivo imaging*

The SCI mice were administered intravenously DiR-labeled PEG-LIP, RM-LIP (0.2 mg/kg) and sacrificed after 1, 4, 8 and 12 h ($n = 3$). The major organs and spinal cord were excised for *ex vivo* imaging using a living imager (BRUKER, FX pro, Germany).

2.8. *Macrophage activation*

RAW264.7 cells were activated as previously reported protocol [25]. To obtain M1 phenotype, RAW264.7 cells were cultured with DMEM complete medium with 25 ng/ml IFNγ and 100 ng/ml LPS for 48 h. For M2 macrophage, cells were induced by DMEM cell medium supplemented with 10 ng/ml IL-4 for 48 h.

2.9. *Quantitative analysis of recognition receptors*

Quantitation of cell surface proteins by flow cytometry was performed according to the previous report [26]. Cells of interest were collected and stained with PE anti-mouse Mac-1 with 0.25 μg per million cells in 100 μl or PE anti-mouse integrin α4 with 1 μg per million cells in 100 μl volume at 4 °C for 30 min. The cells were then washed twice with PBS and finally analyzed using flow cytometry. A Quantum^{TM}R-PE MESF kit was used for the standardization of fluorescence intensity according to the manufacturer's protocol. The kit was comprised of one blank microsphere population and four microsphere populations labeled with increasing amounts of the specified fluorochrome [27]. Firstly, one drop of each of microsphere populations was added to 400 μl suspending

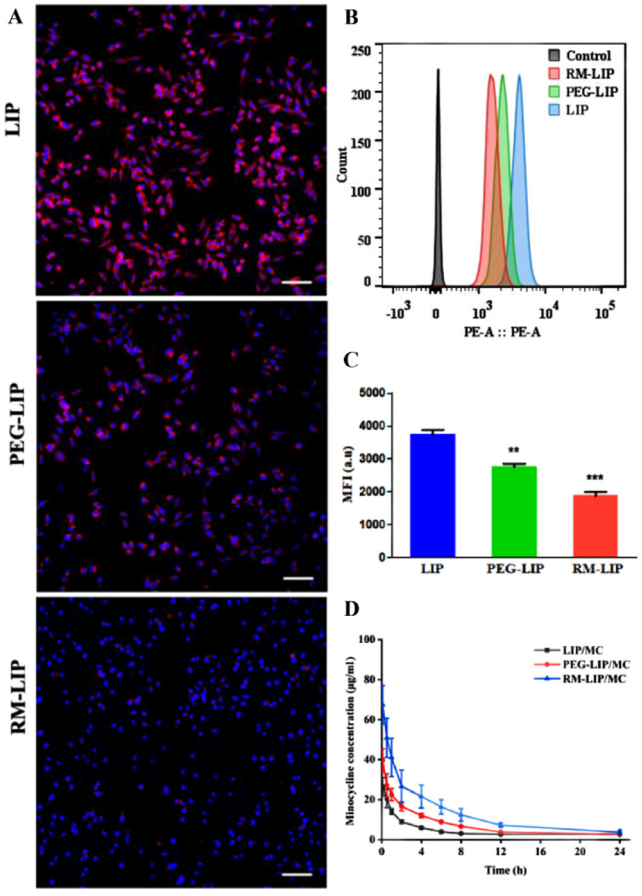

Fig. 3 – The long-circulation performance of RM-LIP *in vitro* and *in vivo*. (A) Cellular uptake of different liposomes in murine macrophage cells-RAW 264.7 under a fluorescence microscope. scale bar, 100 μm; (B) Flow cytometry results of cellular uptake in RAW264.7; (C) Quantification of the mean fluorescence intensity of the flow cytometry histograms ($n = 3$, $^{**}P < 0.005$, $^{***}P < 0.001$); (D) Pharmacokinetics of minocycline-loading liposomes in rats for 24 h after administration ($n = 6$).

solution, respectively, which must be the same type of buffer or medium as stained cells. And then these microspheres were subjected to flow cytometric analysis to establish a calibration curve relating instrument channel values to standardized fluorescence intensity (MESF) units, which can be used to calculate the number of each molecule on the cell surface from the fluorescence intensity.

2.10. *Targeting of nanoparticles coated with different polarized macrophage membranes*

The isolation of M1 RAWMs and M2 RAWMs and the preparation of RM1-LIP and RM2-LIP were the same as RM-LIP. The binding capacity of three formulations to inflamed HUVECs was detected by flow cytometry and fluorescence imaging. The distribution of the three preparations *in vivo* was analyzed by the *in ex* imaging experiments. All operating methods were as described above.

2.11. *Behavioral evaluation*

SCI mice were randomly divided into four groups: saline, free minocycline, PEG-LIP/MC, and RM-LIP/MC. Except for the saline group, which was injected with saline, the rest of each group was administered minocycline (14 mg/kg) every 24 h for 7 days consecutively. Normal mice were set as the control group. Locomotor recovery of mice after SCI was assessed using the Basso Mouse Scale (BMS), as previously described [28]. Recovery of motorfunction was observed and scored by two investigators in a double-blind manner. The scale ranges from 0 (complete hind limb paralysis) to 9 (normal locomotion) based on hind limb motor function [29]. The behavioral assay was performed on days 1, 3, 5, 7, 14, 21, 28, 35, 42 and 49 post-injury.

2.12. *Anti-pyroptosis and anti-inflammatory research*

Mice were sacrificed after the end of treatment. The injured segments of the spinal cord (about 1 cm) were dissected from the mice and weighed. The samples were homogenized with PBS (10 ml/g) and centrifuged at 3000 g for 30 min. The IL-1β and IL-18 concentrations of collected supernatant were analyzed by ELISA kits and the pyroptosis-related proteins, including nod-like receptor family pyrin domain containing 3 (NLRP3), GSDMD-E, GSDMD-N, Caspase-1, and ACS, were measured using western blot. Besides, the concentrations of TNF-α and IL-6 were analyzed using ELISA kits for anti-inflammatory research. Normal mice served as a control.

2.13. *Statistical analysis*

The data were analyzed using GraphPad Prism 8 (GraphPad Software, Inc., La Jolla, CA, USA). Significant differences were evaluated using an unpaired Student's *t*-test for two-group comparisons and one-way ANOVA for a comparison of multiple-group. The data are expressed as the mean ± SD, and $P < 0.05$ was considered statistically significant.

3. Results and discussion

3.1. *Preparation and characterization of RM-LIP*

RM-LIP as a drug delivery platform was prepared by following steps (Scheme 1): (i) synthesis of liposome core (PEG-LIP); (ii) extraction of RAW264.7 membranes (RAWMs); (iii) cloaking PEG-LIP with RAWMs. Compared with PEG-LIP, RM-LIP presented a clear core/shell structure by using TEM (Figs. 2A and S1), indicating the existence of a monolayer membrane coating over the PEG-LIP. The particle size of RM-LIP was 110.08 ± 1.97 nm, slightly greater than that of bare PEG-LIP (77.61 ± 1.78) (Figs. 2B and S2), and complete colocalization of the PEG-LIP core and RAWMs in RM-LIP was observed using a HCS (Fig. 2E). These results demonstrated the successful decoration of PEG-LIP with RAWMs. Only a negligible change in particle size of RM-LIP was observed over 72 h at room temperature, showing its good stability over time (Fig. S3).

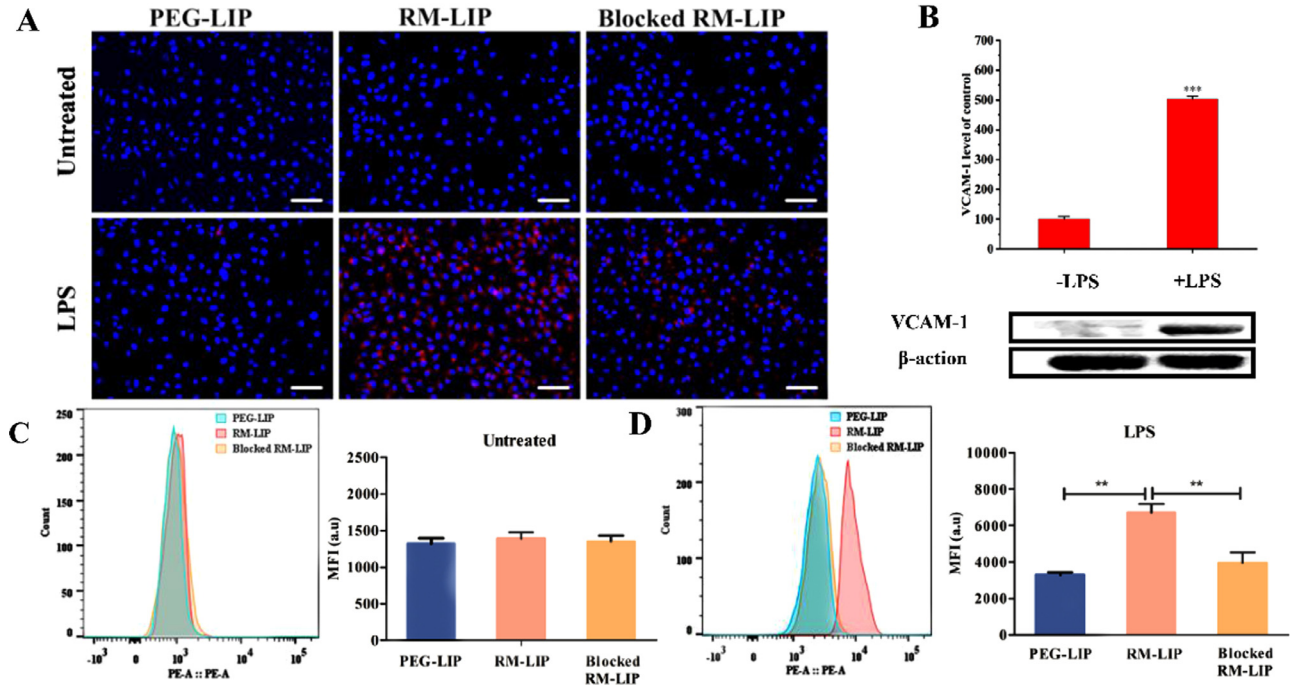

Fig. 4 – The preferential binding of RM-LIP to inflamed endothelial cells *in vitro*. (A) Representative fluorescence images of different liposomes (red) and HUVECs (blue) in the untreated group and the LPS treated group (scale bar: 50 μm). (B) Representative western blots of VCAM-1 from untreated HUVECs and LPS treated HUVECs, and β-actin as an internal reference protein, and quantitative analysis results were presented by a histogram. ($n = 3$, ***$P < 0.001$). Flow cytometry analysis of the binding of RM-LIP to LPS-treated HUVECs (C) and untreated HUVECs (D) ($n = 3$, **$P < 0.005$).

SDS-PAGE analysis indicated that the protein band of the RM-LIP and RAWMs were quite similar, indicating the effective maintaining of RAWMs proteins in RM-LIP (Fig. 2C). Besides, two significant functional proteins, integrin α4 and Mac-1, were confirmed to be maintained in the RM-LIP by western blot (Fig. 2D). RM-LIP/MC was successfully prepared, and the EE of minocycline in the RM-LIP/MC was 91.2%, showing a satisfactory encapsulation ability. *In vitro* drug release study showed that RM-LIP had better sustained-release characteristics than LIP and PEG-LIP (Fig. 2F), which could guarantee minimal leakage of the drug during transport in the circulation.

3.2. *Long cycling performance of RM-LIP*

The therapeutic efficacy of systemic drug-delivery vehicles closely associates with their ability to evade the immune system [23,30]. To confirm that macrophage membrane decoration can reduce the uptake of liposomes by the mononuclear phagocytic system, the cellular uptake of RM-LIP was subjected in RAW 264.7 macrophage cells [31]. As shown in Fig. 3A, the macrophage uptake of RM-LIP was significantly reduced compared with that in other control groups in the same condition. The quantitative results of flowcytometry showed that internalization of RM-LIP in macrophages was reduced by about 26% compared with PEG-LIP, and the reduction was more significant compared with LIP (~50%) (Fig. 3B and 3C).

A pharmacokinetic assay further verified that compared with LIP/MC and PEG-LIP/MC, RM-LIP/MC exhibited longer blood circulation time. The elimination half-time of RM-LIP/MC (13.92 h) was about twice that of PEG-LIP/MC (7.83 h), which means that RM-LIP/MC had more opportunities to accumulate at the target site instead of being directly taken up by the reticuloendothelial system (Fig. 3D and Table S1).

3.3. *In vitro binding to inflamed endothelium*

The main mechanism by which macrophages target sites of SCI is inflammation-induced binding [32]. To explore the binding ability of RM-LIP to inflamed endothelial cells *in vitro*, HUVECs were treated with LPS (1 μg/ml) to induce inflammation, followed by incubation with NiL-labeled RM-LIP and PEG-LIP. Non-treated HUVECs served as controls. Fluorescence microscope images and flow cytometry analysis results displayed that the binding of RM-LIP to LPS-treated HUVECs was significantly higher than that to PEG-LIP, confirming the active binding of RM-LIP to inflamed endothelium (Fig. 4A, 4C and 4D). To further clarify the binding mechanism, blocked RM-LIP was set as a control, whose Mac-1 and integrin α4 proteins had been blocked by related antibodies. The results revealed the binding of blocked RM-LIP to LPS-treated HUVECs was lower than RM-LIP, which demonstrated Mac-1 and integrin α4 play a vital role in the specific binding of RM-LIP to inflamed HUVECs.

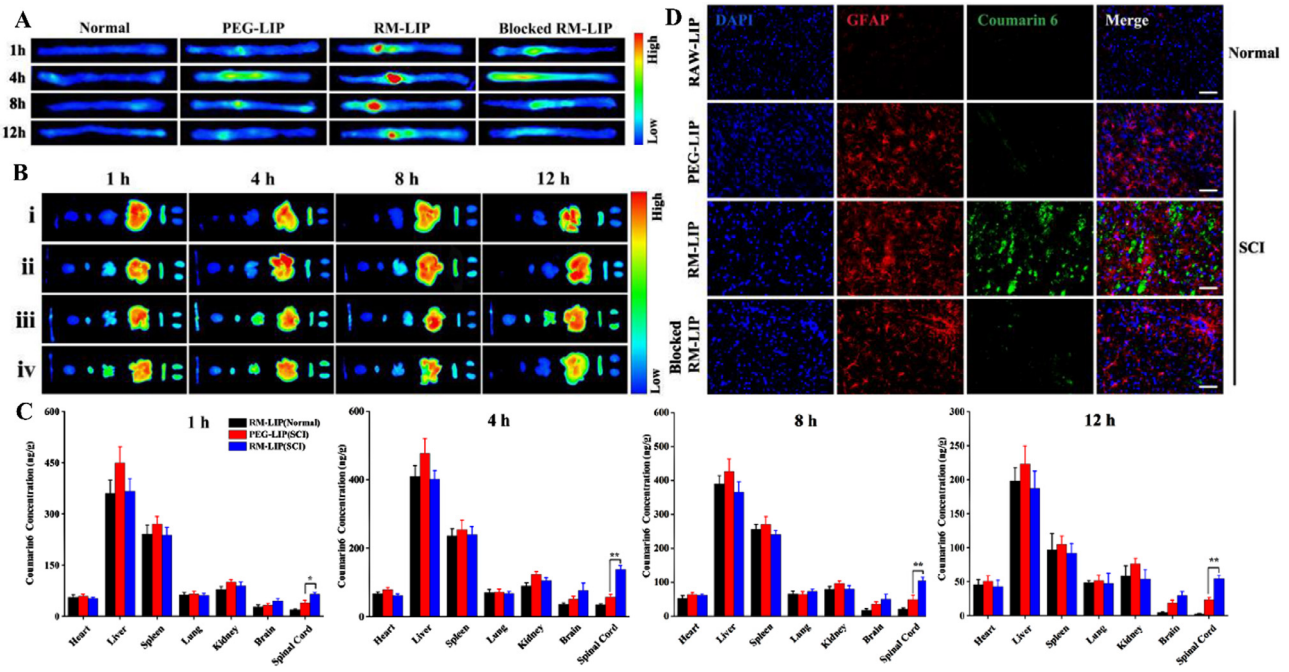

Fig. 5 – Targeting effect of RM-LIP to SCI. (A) and (B) Representative *ex vivo* images of mice 1, 4, 8 and 12 h after injection of DiR-labeled liposomes: normal mice treated with RM-LIP/DiR (i), SCI mice treated with PEG-LIP/DiR (ii), SCI mice treated with RM-LIP/DiR (iii), SCI mice treated with blocked RM-LIP/DiR(iv). The organs were organized in the following order (from left to right): spinal cord, brain, heart, lung, liver, spleen, kidney; (C) Coumarin 6 concentration in various tissues at different time points after intravenous injection of PEG-LIP/C6 and RM-LIP/C6. Data were presented as mean ± SD ($n = 3$, *$P < 0.05$, **$P < 0.005$); (D) Fluorescence images of different liposomes (green) and GFAP (red) in normal spinal cords or injured spinal cords (Scale bar: 100 μm).

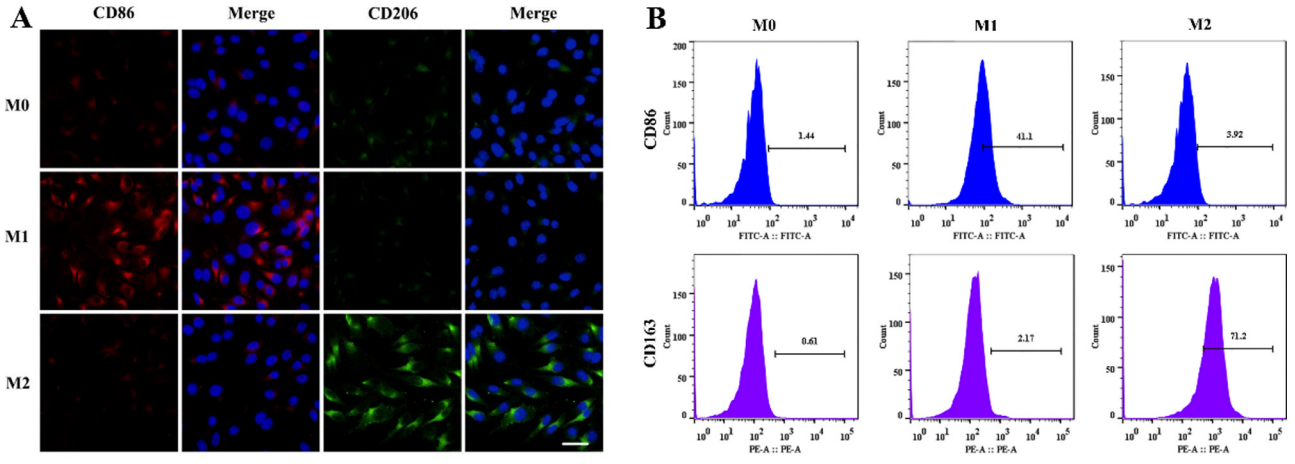

Fig 6 – Characterization of macrophage polarization. (A) Immunofluorescence images of CD86 and CD206 in macrophages (scale bar: 20 μm); (B) Flow cytometry analysis of CD86 and CD163 expressions in macrophages.

There was no distinct difference in the binding of each group to untreated HUVECs, and western blot analysis showed that the expression of VCAM-1 in LPS-treated HUVECs was greatly increased as compared with untreated HUVECs ($P < 0.001$) (Fig. 4B). These results indicated that the active binding of RM-LIP to inflamed HUVECs was attributed to the ligands interactions between VCAM-1 and integrin α4/Mac-1.

3.4. *Targeting SCI*

The targeting of the RM-LIP to the trauma sites of the spinal cord *in vivo* was further detected by using an *in vivo* imaging system and the contusive SCI model was chosen because of its clinical similarity [33]. *Ex vivo* images of spinal cords revealed that compared with other treatment groups, injury sites of SCI mice in the RM-LIP group had remarkably higher fluorescence

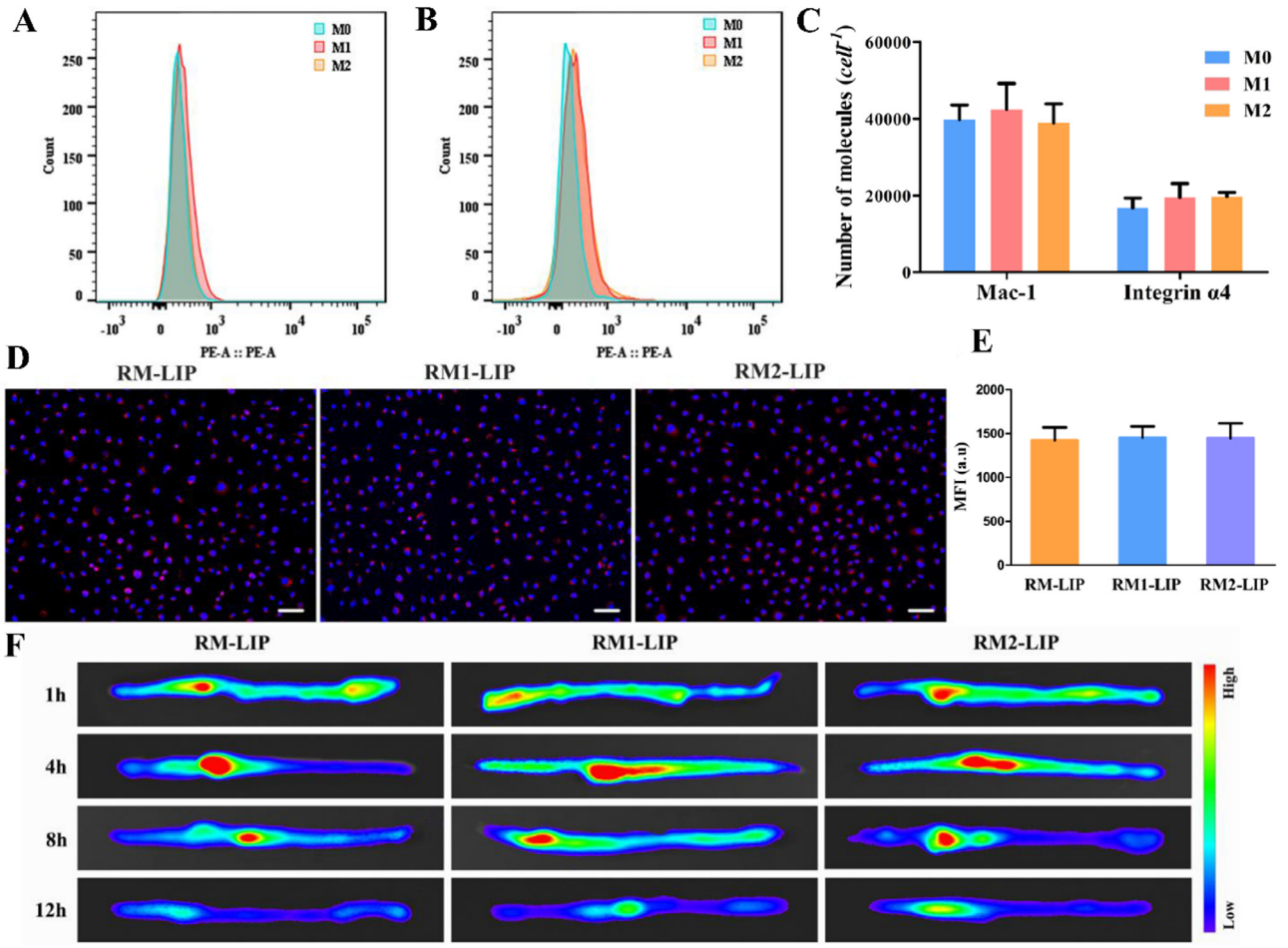

Fig. 7 – The influence of different macrophage polarization states. The expression of Mac-1 (A) and integrin α4 (B) in different macrophage subtypes were analyzed by flow cytometry; (C) The number of Mac-1 and integrin α4 molecules on a cell surface of macrophages by using a QuantumTMR-PE MESF kit to standardizing fluorescence intensity ($n = 3$); (D) Representative fluorescence images of different liposomes (red) and HUVECs (blue) in the LPS-treated HUVECs (scale bar: 50 μm); (E) Quantification of the fluorescence intensity of preparations by using flow cytometry ($n = 3$); (F) Representative ex vivo images of mice in 1, 4, 8 and 12 h after injection of DiR-labeled liposomes: RM-LIP/DiR (i), RM1-LIP/DiR (ii), RM2-LIP/DiR (iii).

signals (Fig. 5A and 5B). When RM-LIP/DiR were injected into normal mice, there was no obvious fluorescence in spinal cords, indicating that RM-LIP can specifically be accumulated at the damaged sites after SCI.

To quantitatively analyze the distribution of liposomes *in vivo*, C6-loaded liposomes were administered to SCI mice and the content of C6 in different tissues was determined by tissue homogenate [34]. The content of C6 at the traumatic sites of the spinal cord in the RM-LIP group was significantly enriched compared to that of the PEG-LIP, especially at 4 h post-administration (Fig. 5C). At this time point, 138 ng C6 per g tissue from RM-LIP was detected in the injured spinal cord, whereas PEG-LIP delivered 58 ng C6 per g tissue. The penetration of preparations in the damaged sites after SCI was evaluated by using a fluorescence microscope. The results indicated that RAWMs encapsulation can help liposomes penetrate the damaged spinal cord. At the same time, RM-LIP/C6 rarely penetrated the normal spinal cord, which demonstrated RM-LIP had great selectivity and safety (Fig. 5D).

3.5. *The influence of different macrophage polarization states*

Unlike most cell membranes, the macrophage membranes inherit the characteristics of their parent cells, with heterogeneity and diversity. Considering that the expression of target receptors of macrophages in different polarization states might be different, which would affect the delivery effects of macrophage membrane-coating nanoparticles, we induced macrophages in different polarization states and analyzed their surface targeted receptors expressions using an absolute quantitative method. Moreover, the delivery effects of different polarized macrophage membrane-modified nanoparticles also were evaluated *in vivo* and *in vitro*. Firstly, we characterized different subtypes of macrophages by analyzing the surface marker proteins and cytokine productions. LPS/IFNγ stimulated macrophages had higher expression of M1 surface markers (CD86) and cytokines (IL-1β and TNF-α), while IL-4 induced macrophages significantly

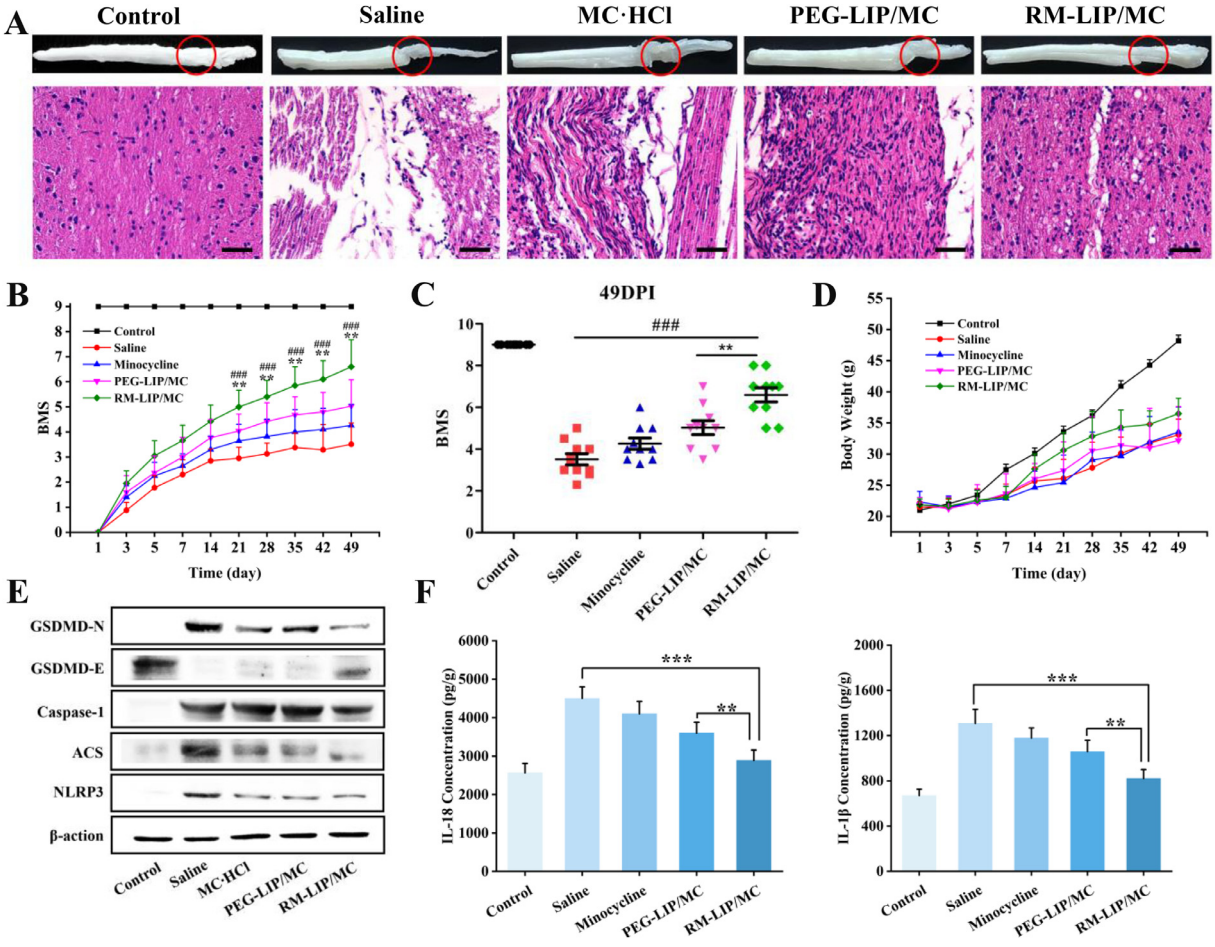

Fig. 8 – The therapeutic effect of RM-MC-LIP on SCI, and the anti-pyroptosis mechanism. (A) H&E staining of spinal cords of each treatment group (scale bar: 50 μm); (B) The BMS scores of SCI mice treated with minocycline, PEG-MC-LIP and RM-MC-LIP, respectively, healthy mice were utilized as Control (BMS score = 9). **$P < 0.005$ *vs.* PEG-MC-LIP group, ###$P < 0.001$ *vs.* Saline group. Data were presented as mean ± SD ($n = 10$); (C) BMS scores of mice at day 49 post-injury; (D) Body weight change of mice ($n = 10$); (E) The expression of GSDMD-N, GSDMD-E, Caspase-1, ACS and NLRP3 were measured using western blot. β-action as the control; (F) The levels of IL-1β and IL-18 production in the injured spinal cord after the end of treatment was measured by ELISA ($n = 6$, **P< 0.005, ***P< 0.001).

increased the levels of M2 marker proteins (CD163 and CD206) and representative cytokines (Arg-1 and IL-10) (Figs. 6 and S4). The results confirmed M1 phenotype and M2 phenotype were successfully induced. Then, the expression of integrin α4 and Mac-1 in three subtypes were compared by flow cytometry and found not statistically significantly different (Fig. 7A and 7B). The number of Mac-1 and integrin α4 was estimated to be approximately 4×10^4 cell^{-1}and 2×10^4 cell^{-1}, respectively (Fig. 7C and S5). This suggests that different polarization states did not significantly affect the expression of the main target receptors on the macrophage membranes. Finally, the SCI-targeting of these macrophage membrane-coated nanoparticles, including RM-LIP, RM1-LIP and RM2-LIP, were tested *in vitro* and *in vivo*. There was no obvious difference between the three kinds of nanoparticles *in vitro* binding study (Fig. 7D-7E) and *ex vivo* imaging experiment (Figs. 7F and S6). These results illustrated that different polarized macrophage membrane-coated nanoparticles possessed similar targeting ability of SCI. In other words, the targeting of RM-LIP for SCI was not affected by the macrophage polarization states. In addition, the pharmacokinetic profiles of the three preparations in rats were also similar (Fig. S7 and Table S1). These results indicated that three different macrophage membrane-coated liposomes have similar targeted drug delivery capabilities for SCI.

3.6. *Therapeutic effect of RM-LIP/MC on SCI and the related mechanisms*

H&E staining revealed the spinal cord of SCI mice treated with saline existed a large area of cavities, and the integrity and continuity of structure were severely damaged. For mice in the RM-LIP/MC group, this condition had significantly improved, exhibited that the volume of the lesion cavity was remarkably reduced, and structure tended to be intact (Fig. 8A). To assess the efficacy of RM-LIP/MC in functional recovery, the BMS scoring system was employed for the praxiological evaluation of experimental mice. The result indicated that the RM-

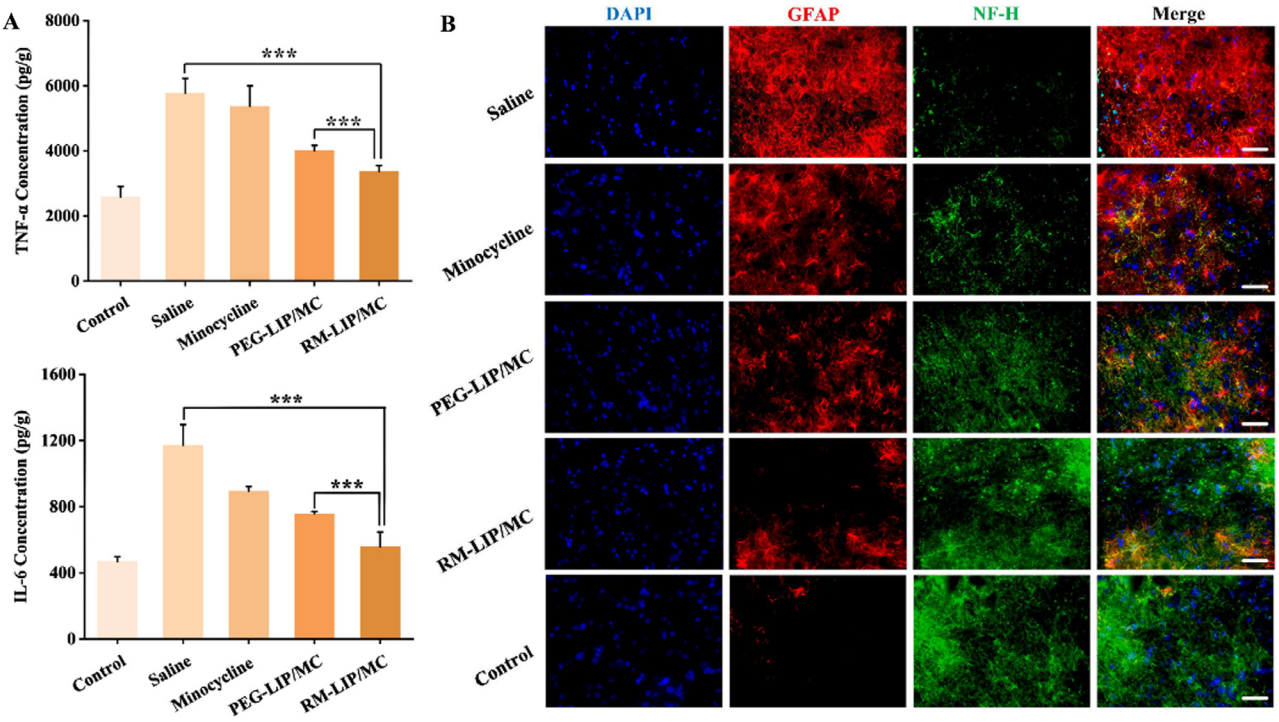

Fig. 9 – The associated mechanisms of RM-LIP/MC in the treatment of SCI. (A) The expression levels of TNF-α and IL-6 in the injured spinal cord after the end of administration. ($n = 6$, **$P < 0.005$, ***$P < 0.001$). (B) Representative fluorescence images of GFAP (red) and NF-H (green) in different groups (scale bar: 50 μm).

LIP/MC group showed a significant increase compared with the other treated groups in the BMS scores beginning 21 days after SCI (Fig. 8B). At 49th day after injury, the BMS score of the RM-LIP/MC group was 1.6 points higher than that of the PEG -LIP/MC group and increased 3.1 BMS score compared to the saline group (RM-LIP/MC: 6.6 ± 1.1; PEG-LIP/MC: 5.0 ± 1.0; saline: 3.5 ± 0.8) (Fig. 8C). The BMS score of 6.6 in the RM-LIP/MC group means consistent plantar stepping and mostly coordination, and the score of 5 in the PEG-LIP/MC group indicates consistent plantar stepping but no coordination, whereas the saline group score of 3.5 represents no or occasional plantar stepping.

As a novel mechanism of cell death, the role of pyroptosis in SCI has gradually attracted attention [35]. In the canonical pyroptosis, pro-caspase-1 and adaptor protein apoptosis-associated speck-like proteins (ASC) are recruited (often by NLRP3) to form inflammasomes. Then, pro-caspase-1 is cleaved to form caspase-1, which not only cleaves pro-IL-1β/18 to form active IL-1β/18 but also cleaves GSDMD into two fragments [36]. The N-terminal fragment (GSDMD-N) damages the cell membrane, which eventually leads to the release of inflammatory factors, cell swelling, and membrane rupture [37]. Therefore, we evaluated the anti-pyroptosis effect of RM-LIP/MC in SCI by analyzing the expression levels of related proteins and cytokines. The western blot analysis revealed the levels of NLRP3, ASC and Caspase-1 in the RM-LIP/MC group were significantly decreased as compared to that of the saline group. At the same time, the upregulation of GSDMD and the downregulation of GSDMD-N in the RM-LIP/MC group were most pronounced among all treatment groups (Fig. 8E). In addition, IL-1β and IL-18 production was significantly decreased in the RM-LIP/MC group (IL-1β: 821.1pg/g, IL-18: 2890.4 pg/g) as compared to the saline group (IL-1β:1308.2 pg/g, IL-18: 4502.1 pg/g) (Fig. 8F).These results indicated that minocycline can exert the anti-pyroptosis effect in SCI by inhibiting the activation of inflammasomes, which was significantly enhanced by the delivery of RM-LIP.

The release of inflammatory mediators (cytokine and chemokines) results in the spreading and exacerbation of tissue injury after SCI [38]. Therefore, the expression levels of two important proinflammatory cytokines TNF-α, IL-6 in traumatic spinal cords were measured. As shown in Fig. 9A, compared with the saline group, other treated groups were found to reduce the expression of these cytokines. Among them, the RM-LIP/MC group (TNF-α: 3361.2 pg/g; IL-6: 558.6 pg/g) had the highest extent of reduction and indicated statistically significant differences compared with the PEG-LIP/MC group (TNF-α: 4005.8 pg/g; IL-6: 757.4 pg/g) (***$P < 0.001$). This result suggested that RM-LIP/MC can effectively reduce the production of inflammatory factors after SCI. Moreover, we additionally evaluated the anti-inflammatory effects of three different macrophage membrane-coated nanoparticles (Fig. S8). The three kinds of drug-loaded nanoparticles all showed obvious effects of inhibiting inflammatory factors, and there was no significant difference between the three treatment groups.

After SCI, reactive astrocytes contribute to the formation of glial scars and limit axonal regeneration [39]. As an acidic

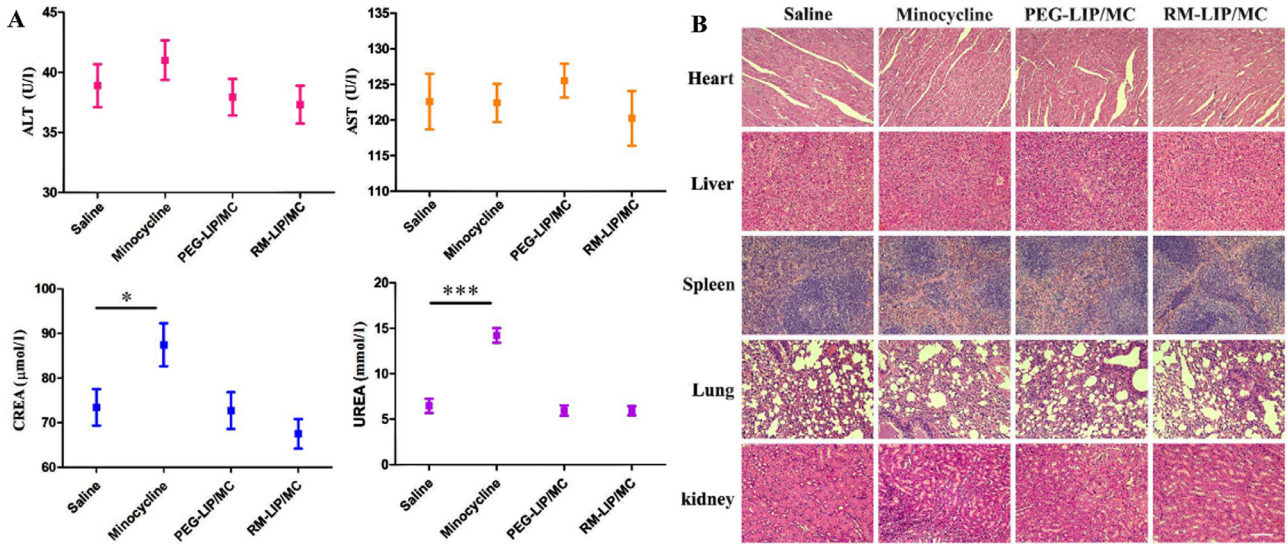

Fig. 10 – Safety of RM-LIP/MC. (A) Main physiological indexes (ALT, AST, CREA and UREA) of mice after treatments of different groups ($n = 3$). (B) H&E staining of main organs in different groups (scale bar: 200 μm).

protein in the cytoplasm, GFAP is often used as a marker for activated astrocytes. NF-H, as a significant neurofilament protein, was used as an axon marker protein. In the injured spinal cord of RM-LIP/MC treated mice, the expression of GFAP was significantly decreased and the level of NF-H was markedly increased as compared to that of the saline group. These results indicated that RM-LIP/MC can suppress the formation of glial scars and reduce axon necrosis (Fig. 9B).

3.7. *Safety evaluation*

According to relevant reports, long-term and high-dose use of minocycline may cause liver and kidney toxicity and even death [40]. To investigate the safety of each preparation, serum biochemical indicators (AST, ALT, CREA, UREA) were tested in mice of all groups. After 7 days of continuous administration, the four biochemical parameters of each group were within normal ranges except the minocycline group (Fig. 10A). H&E staining further revealed that except for the kidney tissue in the minocycline group, no obvious pathological changes in the other groups (Fig. 10B). These results indicated that compared with free minocycline, RM-LIP/MC can significantly reduce liver and kidney toxicity, displaying good biosafety.

4. Conclusion

In this study, macrophage membrane-camouflaged liposomes (RM-LIPs) were innovatively applied to the targeting and treatment of SCI. Specifically, the impact of different macrophage types on the RM-LIP was also explored. The results *in vitro* and *in vivo* demonstrated: (I) The RAWMs-coating could reduce the uptake of the nanoparticles by macrophages and prolonged circulation time *in vivo*; (II) RM-LIP could specifically bind to inflamed endothelial cells and specifically accumulated the injured sites in SCI mice, which was independent of macrophage polarization state; (III) RM-LIP/MC was able to efficiently treat the SCI mice, without any adverse effects. In summary, our study provides a novel biomimetic strategy for treating SCI and considered the influence of cell typing on biomimetic nanoparticles, which provides new ideas for the design of cell-based biomimetic delivery systems.

Conflicts of interest

The authors have declared no conflict of interest.

Acknowledgments

This work was supported by the National Natural Science Foundation of China (No.81673376), the National Natural Science Foundation of Chongqing (cstc2015jcyjBX0100) and the project for innovative Research Group at Higher Educational Institutions in Chongqing (CXQT20006).

Supplementary materials

Supplementary material associated with this article can be found, in the online version, at doi:10.1016/j.ajps.2021.03.005.

REFERENCES

[1] Caron I, Papa S, Rossi F, Forloni G, Veglianese P. Nanovector-mediated drug delivery for spinal cord injury treatment. Wiley Interdiscip Rev 2014;6(5):506–15.
[2] Assinck P, Duncan GJ, Hilton BJ, Plemel JR, Tetzlaff W. Cell transplantation therapy for spinal cord injury. Nat Neurosci 2017;20(5):637–47.

[3] Kabu S, Gao Y, Kwon BK, Labhasetwar V. Drug delivery, cell-based therapies, and tissue engineering approaches for spinal cord injury. J Control Release 2015;219:141–54.
[4] Teng YD, Choi H, Onario RC, Zhu S, Desilets FC, Lan S. Minocycline inhibits contusion-triggered mitochondrial cytochrome c release and mitigates functional deficits after spinal cord injury. Proc Natl Acad Sci USA 2004;101(9):3071–6.
[5] Wang Z, Nong J, Shultz RB, Zhang Z, Kim T, Tom VJ. Local delivery of minocycline from metal ion-assisted self-assembled complexes promotes neuroprotection and functional recovery after spinal cord injury. Biomaterials 2017;112:62–71.
[6] Papa S, Caron I, Erba E, Panini N, De Paola M, Mariani A. Early modulation of pro-inflammatory microglia by minocycline loaded nanoparticles confers long lasting protection after spinal cord injury. Biomaterials 2016;75:13–24.
[7] Cerqueira SR, Oliveira JM, Silva NA, Leite-Almeida H, Ribeiro-Samy S, Almeida A. Microglia response and *in vivo* therapeutic potential of methylprednisolone-loaded dendrimer nanoparticles in spinal cord injury. Small 2013;9(5):738–49.
[8] Parodi A, Quattrocchi N, van de Ven AL, Chiappini C, Evangelopoulos M, Martinez JO. Synthetic nanoparticles functionalized with biomimetic leukocyte membranes possess cell-like functions. Nat Nanotechnol 2013;8(1):61–8.
[9] Xuan M, Shao J, Dai L, Li J, He Q. Macrophage cell membrane camouflaged Au nanoshells for *in vivo* prolonged circulation life and enhanced cancer photothermal therapy. ACS Appl Mater Interfaces 2016;8(15):9610–18.
[10] Li R, He Y, Zhu Y, Jiang L, Zhang S, Qin J. Route to rheumatoid arthritis by macrophage-derived microvesicle-coated nanoparticles. Nano Lett 2019;19(1):124–34.
[11] Ji W, Zhang T, Lu Z, Shen J, Xiao Z, Zhang X. Synthesis and characterization of novel biocompatible nanocapsules encapsulated lily fragrance. Chinese Chem Lett 2019;30:739–42.
[12] Hu CMJ, Zhang L, Aryal S, Cheung C, Fang RH, Zhang LF. Erythrocyte membrane-camouflaged polymeric nanoparticles as a biomimetic delivery platform. Proc Natl Acad Sci USA 2011;108(27):10980–5.
[13] He H, Guo C, Wang J, Korzun WJ, Wang X, Ghosh S. Leutusome: a biomimetic nanoplatform integrating plasma membrane components of leukocytes and tumor cells for remarkably enhanced solid tumor homing. Nano Lett 2018;18(10):6164–74.
[14] Hu CM, Fang RH, Wang KC, Luk BT, Thamphiwatana S, Dehaini D. Nanoparticle biointerfacing by platelet membrane cloaking. Nature 2015;526(7571):118–21.
[15] Engelhardt B, Ransohoff RM. Capture, crawl, cross: the T cell code to breach the blood-brain barriers. Trends Immunol 2012;33(12):579–89.
[16] David S, Kroner A. Repertoire of microglial and macrophage responses after spinal cord injury. Nat Rev Neurosci 2011;12(7):388–99.
[17] Murray PJ. Macrophage polarization. Annu Rev Physiol 2017;79:541–66.
[18] Biswas SK, Mantovani A. Macrophage plasticity and interaction with lymphocyte subsets: cancer as a paradigm. Nat Immunol 2010:889–96.
[19] Nie W, Wu G, Zhang J, Huang LL, Ding J, Jiang A. Responsive exosome nano-bioconjugates for synergistic cancer therapy. Angew Chem Int Ed Engl 2020;59(5):2018–22.
[20] Wang C, Wang Y, Zhang L, Miron RJ, Liang J, Shi M. Pretreated macrophage-membrane-coated gold nanocages for precise drug delivery for treatment of bacterial infections. Adv Mater 2018;30(46):e1804023.
[21] Cao H, Dan Z, He X, Zhang Z, Yu H, Yin Q. Liposomes coated with isolated macrophage membrane can target lung metastasis of breast cancer. ACS Nano 2016;10(8):7738–48.
[22] Xing CH, Levchenko T, Guo SZ, Stins M, Torchilin VP, Lo EH. Delivering minocycline into brain endothelial cells with liposome-based technology. J Cereb Blood Flow Metab 2012;32(6):983–8.
[23] Tang Y, Wang X, Li J, Nie Y, Liao G, Yu Y. Overcoming the reticuloendothelial system barrier to drug delivery with a "don't-eat-us" strategy. ACS Nano 2019;13(11):13015–26.
[24] Allen TM, Sapra P, Moase E. Use of the post-insertion method for the formation of ligand-coupled liposomes. Cell Mol Biol Lett 2002;7:889–94.
[25] Qie Y, Yuan H, Von Roemeling CA, Chen Y, Liu X, Shih KD. Surface modification of nanoparticles enables selective evasion of phagocytic clearance by distinct macrophage phenotypes. Sci Rep 2016;6:26269.
[26] Ito T, Kumagai Y, Itano K, Maruyama T, Tamura K, Kawasaki S. Mathematical analysis of gefitinib resistance of lung adenocarcinoma caused by MET amplification. Biochem Biophys Res Commun 2019;511(3):544–50.
[27] Serke S, Lessen AV, Huhn D. Quantitative fluorescence flow cytometry: a comparison of the three techniques for direct and indirect immunofluorescence. Cytometry 1998;33(2):179–87.
[28] Basso DM, Fisher LC, Anderson AJ, Jakeman LB, Mctigue DM, Popovich PG. Basso mouse scale for locomotion detects differences in recovery after spinal cord injury in five common mouse strains. J Neurotrauma 2006;23:635–59.
[29] Tang P, Zhang Y, Chen C, Ji X, Ju F, Liu X. *In vivo* two-photon imaging of axonal dieback, blood flow, and calcium influx with methylprednisolone therapy after spinal cord injury. Sci Rep 2015;5:9691.
[30] Rao L, Bu LL, Xu JH, Cai B, Yu GT, Yu X. Red blood cell membrane as a biomimetic nanocoating for prolonged circulation time and reduced accelerated blood clearance. Small 2015;11(46):6225–36.
[31] Jain NK, Mishra V, Mehra NK. Targeted drug delivery to macrophages. Expert Opin Drug Deliv 2013;10(3):353–67.
[32] Shechter R, Miller O, Yovel G, Rosenzweig N, London A, Ruckh J. Recruitment of beneficial M2 macrophages to injured spinal cord is orchestrated by remote brain choroid plexus. Immunity 2013;38(3):555–69.
[33] Silva NA, Sousa N, Reis RL, Salgado AJ. From basics to clinical: a comprehensive review on spinal cord injury. Prog Neurobiol 2014;114:25–57.
[34] Xu Y, Tian M, Zhang H, Xiao Y, Hong X, Sun Y. Recent development on peptide-based probes for multifunctional biomedical imaging. Chinese Chemical Letters 2018;29(7):1093–7.
[35] Al Mamun A, Wu Y, Monalisa I, Jia C, Zhou K, Munir F. Role of pyroptosis in spinal cord injury and its therapeutic implications. J Adv Res 2021;28:97–109.
[36] Tsuchiya K. Inflammasome-associated cell death: pyroptosis, apoptosis, and physiological implications. Microbiol Immunol 2020;64(4):252–69.
[37] Hu X, Chen H, Xu H, Wu Y, Wu C, Jia C. Role of pyroptosis in traumatic brain and spinal cord injuries. Int J Biol Sci 2020;16(12):2042–50.
[38] Rawji KS, Mishra MK, Michaels NJ, Serge R, Stys PK, Yong VW. Immunosenescence of microglia and macrophages: impact on the ageing central nervous system. Brain 2016;139:653–61.
[39] Zhao YY, Yuan Y, Chen Y, Jiang L, Liao RJ, Wang L. Histamine promotes locomotion recovery after spinal cord hemisection via inhibiting astrocytic scar formation. CNS Neurosci Ther 2015;21(5):454–62.
[40] Urban TJ, Nicoletti P, Chalasani N, Serrano J, Stolz A, Daly AK. Minocycline hepatotoxicity: clinical characterization and identification of HLA-B*35:02 as a risk factor. J Hepatol 2017;67(1):137–44.